Bioorganic & Medicinal Chemistry 19 (2011) 2478–2484

Contents lists available at ScienceDirect

Bioorganic & Medicinal Chemistry

journal homepage: www.elsevier.com/locate/bmc

5′-Modified pyrimidine nucleosides as inhibitors of ribonuclease A

Anirban Samanta, Swagata Dasgupta *, Tanmaya Pathak *

Department of Chemistry, Indian Institute of Technology, Kharagpur 721302, India

ARTICLE INFO

Article history:
Received 3 June 2010
Revised 27 August 2010
Accepted 28 August 2010
Available online 21 March 2011

Keywords:
Ribonuclease A
Aminonucleoside
Inhibition

ABSTRACT

Four 5′-deoxy-5′-nipecotic acid substituted pyrimidine nucleosides were synthesized and characterized. Their inhibitory activities towards ribonuclease A (RNase A) have been studied by enzyme kinetics and docking experiments. All inhibition constants obtained were in the sub-millimolar range. Biochemical analysis shows that the uridine derivative is more potent than the corresponding thymidine derivatives and that the inhibition is competitive in nature. For thymidine derivatives, the 3′-hydroxy group plays an important role in binding as well as in inhibition. Docking studies also support the experimental results. In the docking conformation the uridine derivative was found to bind to the P_1P_2 subsite with the acid group within hydrogen bonding distance of the active site histidine residues.

1. Introduction

Specific members of the RNase A superfamily have received increased attention since they are able to exhibit cytotoxic and angiogenic properties.[1–3] Several chemical modification and site-directed mutagenesis experiments reveal that the ribonucleolytic activity of these proteins are responsible in most of the cases for their physiological actions.[4–7] These studies suggest that their biological activity critically depend on the cleavage of RNA which is encouraging for new routes of treatment of various diseases. Inhibitors of such enzymatic activity could be useful as potential drug molecules.[8] Structure-assisted inhibitor design strategies have mainly focused on RNase A due to the high degree of conservation of the active site among the members of this superfamily.

RNase A is an endonuclease that cleaves RNA in two steps—by transphosphorylation and hydrolysis reactions.[9] Various subsites exist within the central catalytic groove of RNase A, where the substrate, RNA binds. These are defined as $P_0\cdots Pn$, $R_0\cdots Rn$, and $B_0\cdots Bn$ which are the binding sites for the phosphate, ribose and the nucleobase respectively of the natural substrate RNA (n indicates the position of the group with respect to the cleaved phosphate phosphodiester bond where $n = 1$). In all RNases the main subsite P_1 is conserved, whereas subsites B_1 and B_2 on each side of P_1 are partially conserved.[10] Nevertheless, B_1 binds pyrimidines, while B_2 has a strong base preference for purines.

Several nucleoside-based inhibitors of RNase A functionalized with phosphate or pyrophosphate, which are substrate mimics inhibit the ribonucleolytic activity of the enzyme effectively.[8,10] The best synthetic inhibitor of RNase A identified till date is pdUppA-3′-p ($K_i = 27$ nM).[11] The utility of these nucleotides as inhibitors is, however, limited. The problem associated with these compounds is their inherent metabolic instability, as the free phosphate groups are susceptible to dephosphorylation by phosphatases which markedly diminish their potency.[11] Moreover, the high negative charge on the phosphate groups makes them difficult to use in vivo because the transport of these molecules across biological membranes is hindered.[8]

The pK_a values of histidine residues present in the active site (His12 and His119) of RNase A changes from ~5.22/6.78 for the free enzymes to ~6.30/8.10 in case of the enzyme–substrate complex.[12] Aminonucleosides with amino groups that have basicities comparable to those of the imidazole of His12 and His119 are able to perturb the protonating/deprotonating environment of the P_1 site.[13] At physiological pH, inhibitors with acidic moieties would exist in the deprotonated form and would therefore interact electrostatically with the protonated basic groups present at the P_1 subsite.[13] This would in turn affect the ribonucleolytic activity of RNase A as the cationic histidine residues contribute significantly to the stability of the RNase A-single stranded nucleic acid complex through Coulombic interactions with the anionic phosphoryl groups of the nucleic acid.[14]

A few 3′- and 5′-modified aminonucleosides with varying pK_a values of amines,[13] nucleoside-amino acid[15] and nucleoside-dibasic acid[16] conjugates have been reported from our laboratory. These inhibitors show varying inhibitory potency due to different binding patterns as observed in the docking studies and crystallographic studies.[17,18] The crystallographic studies show that the anchoring point for all six inhibitors is the pyrimidine base which binds at subsite B_1 in the same manner. The 2′-hydroxyl group of 5′-deoxy-5′-*N*-morpholino-, -piperidino-, -pyrrolidino-modified uridine aminonucleosides participates in hydrogen-bond interactions

* Corresponding authors. Tel.: +91 3222 283306 (S.D.); tel.: +91 3222 283342 (T.P.).
E-mail addresses: swagata@iitkgp.ac.in (S. Dasgupta), tpathak@iitkgp.ac.in (T. Pathak).

0968-0896/$ - see front matter © 2010 Published by Elsevier Ltd.
doi:10.1016/j.bmc.2010.08.059

with the side chain atoms of P_1 residues His12 and Lys41. Furthermore, the 3′-hydroxyl group of these compounds is also involved in interactions with His119 and Phe120 (Fig. 1A). The 3′-hydroxyl group of 5′-deoxy-5′-*N*-piperidino-, -pyrrolidino-thymidines participates in hydrogen bonding to His119 and Lys41. The 5′-substituent of these compounds points away from the active site (Fig. 1B).[18] Moreover, the crystal structure of RNase A-3′-nipecotic acid modified *ara*-uridine complex indicates that the acid group becomes an alternative recognition site by binding at subsite B_1 other than the nucleobase but both the free hydroxyl groups are not within hydrogen bonding distance (Fig. 1C).[17]

Molecular recognition being the basis for all biological processes, it is logical to consider that molecules with both hydroxyl groups in addition to the carboxylic moiety would possess greater ribonucleolytic inhibitory potency. Compounds were chosen in a manner such that the role of the hydroxyl group could be identified and the configuration of the hydroxyl group considered. Thus, the synthesis and biological evaluation of 5′-modified uridine nucleosides having 2′,3′-hydroxyl groups, thymidine with 3′-hydroxyl group and thymidine analogues having 3′-β-hydroxy and 2′,3′-didehydro-3′-dideoxy groups were conducted. Agarose gel electrophoresis studies, enzyme kinetics and docking studies were performed to evaluate the inhibitory power and possible interactions.

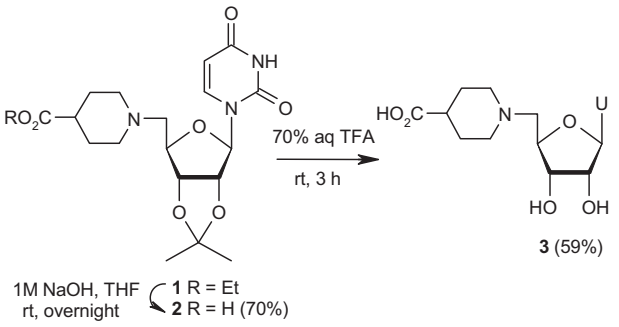

Scheme 1.

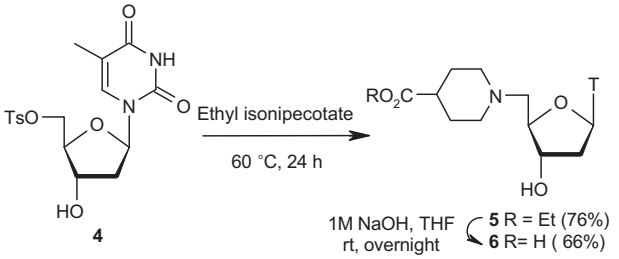

Scheme 2.

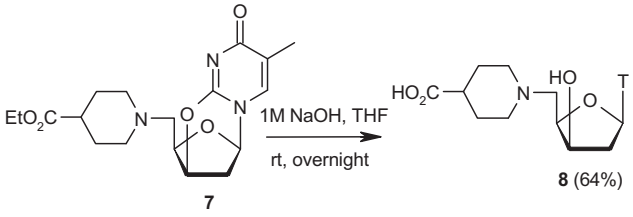

Scheme 3.

2. Results and discussion

2.1. Chemistry

Compound **3** was synthesized from compound **1**[18] by base hydrolysis followed by the treatment of aq TFA (70%) in overall 41% yield (Scheme 1). 5′-*O*-Tosylthymidine **4**[19] was heated with neat ethyl *iso*nipecotate at 60 °C to synthesize compound **5** which on base hydrolysis afforded compound **6** (Scheme 2). 3′,5′-Di-*O*-mesylthymidine was treated with neat ethyl *iso*nipecotate for 2 days at room temperature to afford the known 2,3′-*O*-anhydro compound **7**[20] which was further subjected to base hydrolysis to produce β-hydroxy compound **8** in 64% yield (Scheme 3). In the presence of NaOH, a hard base, the anhydro ring was opened selectively at the C-2 position as it preferentially attacked the sp^2 aromatic C-2 position rather than the softer 3′-position. 5′-*O*-tosyl D_4T **9**[21,22] was stirred with neat ethyl *iso*nipecotate at 60 °C for 24 h to form compound **10** in 86% yield which on base hydrolysis produced compound **11** (Scheme 4).

2.2. Biology

The inhibitory activity of the synthesized compounds against RNase A was initially studied by the agarose gel-based assay. In the agarose gel, bands in lane 1 showed maximum intensity due to presence of control tRNA (Fig. 2). Due to the degradation of tRNA

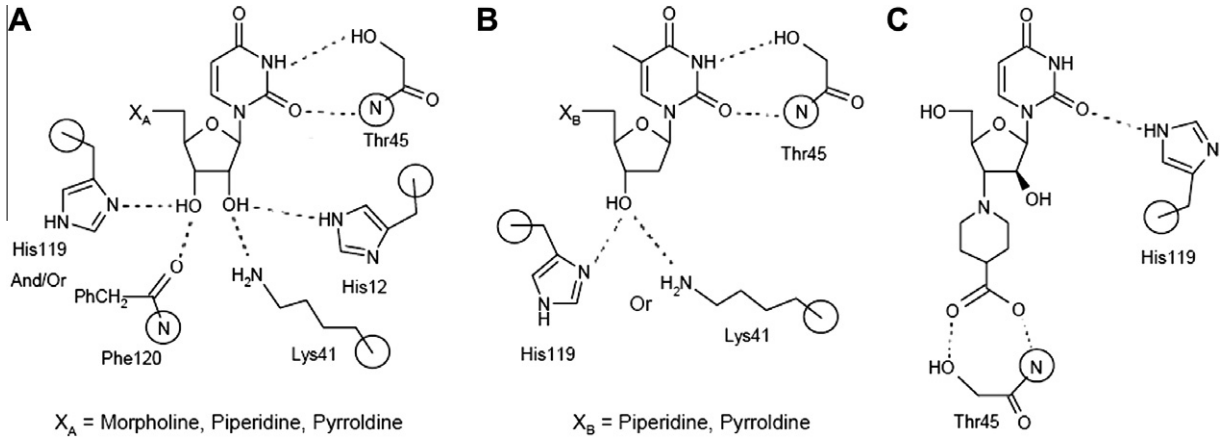

Figure 1. Schematic representation of the hydrogen bonds of RNase A with (A) 5′-aminouridine nucleosides, (B) 5′-aminothymidine nucleosides and (C) 3′-*N*-piperidine-4-carboxyl-3′-deoxy-*ara*-uridine in crystal structure.

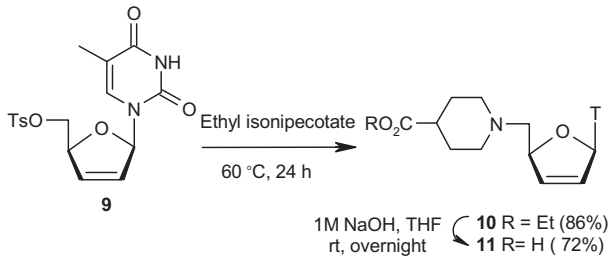

Scheme 4.

Figure 2. Agarose gel based assay for the inhibition of RNase A (1.26 μM): (lane 1) tRNA; (lane 2) tRNA and RNase A; (lanes 3, 4, and 5) tRNA, RNase A and **3**, **6**, **8**, and **11** (0.09 mM, 0.18 mM, and 0.27 mM, respectively).

by RNase A, the band in lane 2 was the least intense. Lanes 3, 4, and 5 of each gel contained tRNA and RNase A with increasing concentrations of synthesized compounds **3**, **6**, **8**, and **11**. The difference in intensity between lanes 2 and 3 was more for compound **3** and these differences gradually increased in lanes 4 and 5. For compounds **6** and **8**, the intensity differences in lanes 3, 4, and 5 with lane 2 were comparable. This intensity change was less prominent for compound **11**.

The inhibition of ribonucleolytic activity of compounds **3**, **6**, **8**, and **11** was further assessed by the precipitation assay (Fig. 3). The inhibition of the ribonucleolytic activity by these compounds for RNase A at the same concentration (0.32 mM) was compared. The activity of RNase A was reduced by 37% by compound **3** while compound **6** showed 23% reduction of ribonucleolytic activity. The

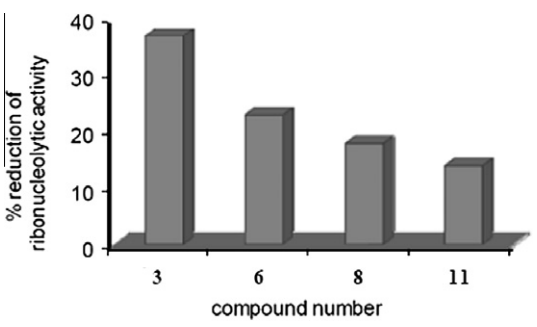

Figure 3. Reduction of ribonucleolytic activity of RNase A (1.26 μM) in the presence of compounds **3**, **6**, **8**, and **11** (0.27 mM) by precipitation assay.

β-hydroxy compound **8** had 18% inhibitory activity. Compound **11** showed comparatively less inhibition of the ribonucleolytic activity (14%) compared to the other acid derivatives. From the above observations, it is apparent that the inhibitory activity was maximum for compound **3** whereas compound **11** was the least potent. The inhibition potency of compounds **6** and **8** were comparable.

For determination of the inhibition constants by kinetic experiments, the reciprocal of reaction velocity was plotted against inhibitor concentration for three different substrate concentrations in the linear Dixon plot. The nature of the plots is indicative of competitive inhibition. The Dixon plot is used for the determination of inhibition constants of competitive inhibitors as it is convenient to directly evaluate the inhibition constant (K_i) from kinetic data. In such cases, when the binding of inhibitor to the enzyme does affect substrate binding or vice versa, Dixon plots may not be used to differentiate between competitive and non-competitive inhibitors.[23] Steady state kinetic experiments were again performed with varying inhibitor concentrations and a Lineweaver–Burk plot obtained with compounds **3**, **6**, **8**, and **11** and the inhibition constants recalculated. The nature of the plots confirms a competitive mode of inhibition. The Dixon and Lineweaver–Burk plots of compound **3** are given in Figure 4(A) and (B), respectively. A comparison with the calculated K_i values from both the Dixon plots and the Lineweaver–Burk plots (Table 1) indicates that compound **3** was more potent than compounds **6**, **8**, and **11** as observed from the precipitation assay.

2.3. Docking studies

In the docking studies, we have attempted to explain the inhibitory activity of these compounds by considering possible modes of binding with RNase A (1FS3). In the docked conformation, compounds **3** and **6** bind at subsite P_1 in an almost similar fashion but compounds **8** and **11** bind away from this subsite. The acid moiety of the 5′-substituent of compound **3** was within hydrogen bonding distance of active site residues His119, Gln11, and His12 (Fig. 5A). The uracil base was also found to be within hydrogen bonding distance of Gln11 of subsite P_1 and Lys7 and Arg10 of subsite P_2. Similarly, compound **6** indicated an interaction through the acid group and the thymine base (Fig. 5B). Here the acid group was close to active site His12 and Lys41 but away from His119 and the thymine nucleobase interacted with only Lys7 and Arg10. The 3′-hydroxyl group of this compound was within hydrogen bonding distance of Arg39. Compound **8** interacted with the enzyme through the nucleobase in the docked structure whereas the 5′-substituent bound away from it (Fig. 5C). The O4 of thymine base was close to Arg10 and O2 was within the hydrogen bonding distance of Lys7 and Gln11. There was also a binding of 3′-β-hydroxyl group of compound **8** with Lys7. The docked conformation of compound **11** showed that the thymine base was close to Arg10 and Lys7 of subsite P_2 but the acid moiety bound away from the active histidine residues of subsite P_1 (Fig. 5D).

In the docked conformation of compound **3**, it appeared that the 2′- and 3′-hydroxyl groups did not take part in any kind of interaction with RNase A. So 2′,3′-*O*-*iso*propylidineuridine compound **2** and compound **3** should show similar activity. But a comparative agarose gel based assay (Fig. 6) revealed that compound **3** was a more potent inhibitor than compound **2**. The docking experiment with compound **2** also showed that the 5′-substituent of this compound was far away from the active site histidine residues (Fig. 7). However the 3′-hydroxyl groups of compounds **6** and **8** play an important role in recognition. The possible hydrogen bonding interaction of the 3′-hydroxyl group of compound **6** with Arg39 (which is close to the active site residues) is responsible for the interaction with the active site P_1. However, the interaction of the 3′-β-hydroxyl group of compound **8** with Lys7 of subsite P_2

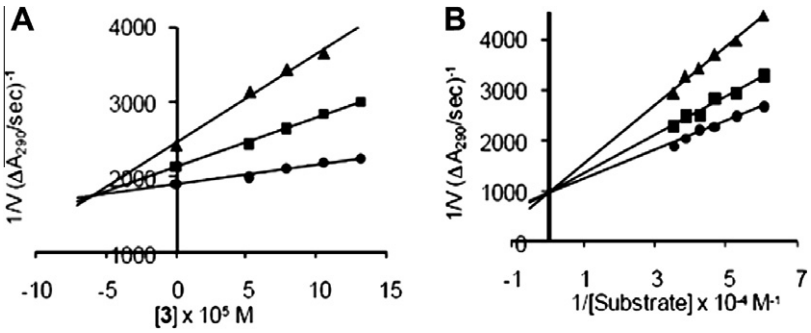

Figure 4. (A) Dixon plots for inhibition of RNase A by compound **3** (0–0.13 mM), 2′,3′-cCMP concentrations of 0.12 (▲), 0.18 (■), 0.24 (●) mM and RNase A concentration of 0.98 μM. (B) Lineweaver–Burk plots for inhibition of RNase A by compound **3** of 0.08 (▲), 0.03 (■), 0 (●) mM, 2′,3′-cCMP concentrations (0.29–0.17 mM) and RNase A concentration of 0.99 μM. Calculated K_i values are listed in Table 1.

Table 1
Inhibition constants (K_i) of the inhibitors

Inhibitor	K_i (μM)	
	Dixon plot	Lineweaver–Burk plot
3	61 ± 3	75 ± 2
6	121 ± 2	162 ± 6
8	183 ± 3	229 ± 7
11	—	250 ± 10

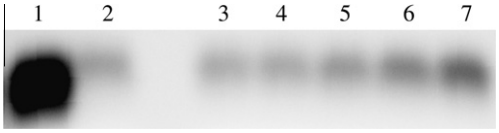

Figure 6. Comparative agarose gel based assay for the inhibition of RNase A. Lane 1: tRNA; lane 2: tRNA and RNase A (1.26 μM); lanes 3, 4, and 5: tRNA, RNase A with compound **2** (0.09 mM, 0.18 mM, and 0.27 mM, respectively), and lanes 6 and 7: tRNA, RNase A with compound **3** (0.18 mM and 0.27 mM, respectively).

could create hindrance for the close proximity to subsite P_1 (Fig. 5C). In all probability, this unfavorable binding with 3′-β-hydroxyl group of compound **8** renders it a weaker inhibitor compared to compound **6**. Compound **11** interacted through the thymine base rather than the acid group of the 5′-substituent as it lacks 3′-hydroxyl group. This pattern of binding might be cause of the lower potency of compound **11** compared to compounds **3**, **6**, and **8**.

For rationalizing the docking experiments, the merged structures of the complexes comprised of the protein and compounds were further analyzed with *PEARLS* (Program of Energetic Analysis of Receptor Ligand System)[24] to determine the '*Receptor–Ligand Internal Energy*.' From this value, the equilibrium constant (K) is calculated for each inhibitor according to $\Delta G = -RT\ln K$. K values obtained from *PEARLS* have been plotted against the experimental inhibition constant values of each inhibitor. From Figure 8 it is observed that there is a positive correlation between the experimental K_i and theoretically obtained K value ($R^2 = 0.887$).

3. Conclusion

Several synthetic 5′-modified aminopyrimidines carrying free carboxylic acid group have been identified as RNase A inhibitors for the first time. Experimental results show that uridine derivative is more potent than the corresponding thymidine derivatives. In docking studies, the acid group of the 5′-modified uridine derivative projected itself to the active site P_1 suggesting efficient binding of this molecule with the active site of RNase A compared to the other thymidine compounds. Between the thymidine inhibitors the acid group of the 5′-modified thymidine derivative is also within hydrogen bonding distance to the active site histidine residues but that of 3′-β-hydroxy thymidine and 2′,3′-dideoxy thymidine derivatives is away from the active site. Interestingly, the binding of thymidine derivatives is directed by the position of 3′-hydroxy group rather than the nucleobase and the acid group. These observations are in line with the experimental data. Inhibitors having an acid moiety could be an alternative anchoring site of a nucleobase

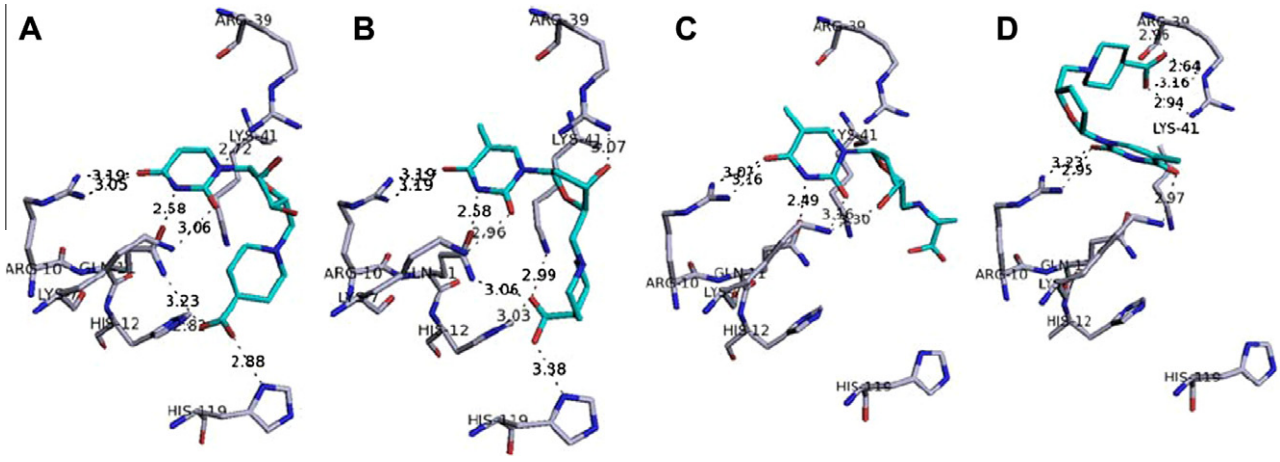

Figure 5. Docked poses of (A) compound **3**, (B) compound **6**, (C) compound **8**, and (D) compound **11** with RNase A (1FS3).

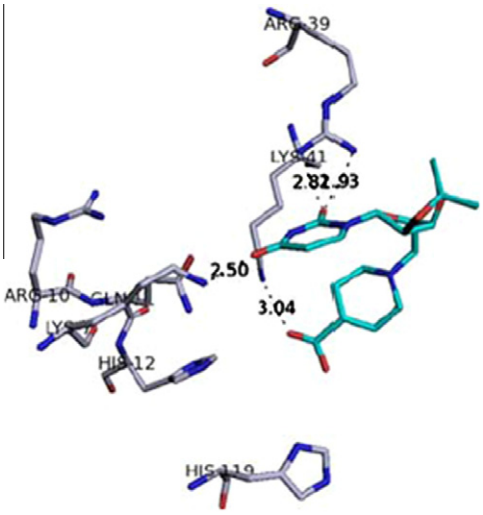

Figure 7. Docked pose of compound **2** with RNase A (1FS3).

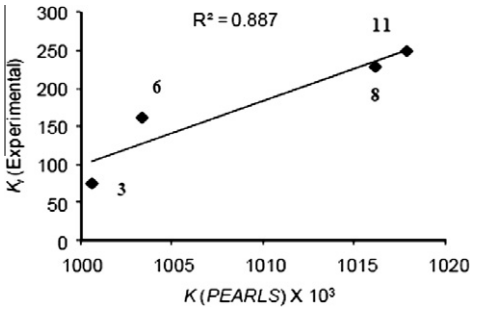

Figure 8. Plot of K_i (experimental) versus K (calculated from *PEARLS*) for inhibitors **3**, **6**, **8**, and **11**.

and this anchoring pattern depends mostly on the structure of the whole molecule rather than the individual functional groups. It appears therefore that slight modifications in the structures of nucleoside-based inhibitors can have a direct impact on their mode of binding with the active sites of RNase A. Further design is likely to result in lead compounds that may be developed for efficient inhibition of the ribonucleolytic activity of members of the RNase superfamily that possess biological activity related to their enzyme activities.

4. Experimental section

4.1. Chemistry

4.1.1. Materials and general methods

Ethyl *iso*nipecotate was purchased from Sigma–Aldrich and all other reagents were from SRL India. Column chromatographic separations were done using silica gel (60–120 and 230–400 mesh). Solvents were dried and distilled following standard procedures. TLC was carried out on precoated plates (Merck silica gel 60, f_{254}) and the spots were visualized with UV light or by charring the plates dipped in 5% H_2SO_4–MeOH solution or 5% H_2SO_4/vanillin/EtOH or 5% ninhydrin in MeOH solution. ^{1}H NMR (400 MHz) and ^{13}C NMR (100 MHz) spectra were recorded on Bruker NMR instrument unless stated otherwise. All ^{1}H NMR in D_2O were recorded using CH_3CN as internal standard. All ^{13}C NMR spectra in D_2O were recorded using DMSO-d_6 as internal standard. Chemical shifts are reported in parts per million (ppm, δ scale). DEPT experiments have been carried out to identify the methylene carbons. Melting points were determined in open-end capillary tubes and are uncorrected.

4.1.2. 5′-Deoxy-5′-N-(4-carboxypiperidinyl)-2′,3′-O-isopropylidineuridine 2

A mixture of compound **1**[18] (0.48 g, 1.13 mmol), THF (10 mL) and aq NaOH (1 M, 10 mL) was stirred overnight. Volatile matters were removed under reduced pressure and the solution was neutralized carefully with aq HCl (1 M). The solvent was removed under reduced pressure and the residue was dissolved in MeOH (3 mL). It was then preadsorbed onto silica gel, applied on the top of the silica gel column, and chromatographed to obtain compound **2** (0.31 g, 70%). [Eluent: 5–20% of MeOH in $CHCl_3$]. Hygroscopic solid. ^{1}H NMR (DMSO-d_6): δ 1.10–1.14 (m, $N(CH_2CH_3)_3$), 1.26 (s, 3H), 1.45–1.55 (m, 5H), 1.72–1.75 (m, 2H), 1.99–2.17 (m, 3H), 2.43–2.55 (m, 2H), 2.75–2.81 (m, 2H), 2.88–2.93 (m, $N(CH_2CH_3)_3$), 4.08–4.12 (m, 1H), 4.61–4.63 (m, 1H), 4.94–4.96 (m, 1H), 5.60 (d, J = 8.0 Hz, 1H), 5.72 (d, J = 1.6 Hz, 1H), 7.77 (d, J = 8.0 Hz, 1H). ^{13}C NMR (DMSO-d_6): δ 9.0 ($N(CH_2CH_3)_3$), 25.6, 27.4, 28.3 (CH_2), 40.4, 45.7 ($N(CH_2CH_3)_3$), 53.1 (CH_2), 53.2 (CH_2), 60.3 (CH_2), 82.7, 83.8, 84.3, 92.3, 102.0, 113.6 (C), 143.0, 150.6 (C), 163.6 (C), 176.4 (C). HRMS (ES^+), m/z calcd for $(M+Na)^+$ $C_{18}H_{25}N_3O_7Na$: 418.1595, found: 418.1591.

4.1.3. 5′-Deoxy-5′-N-(4-carboxypiperidinyl)uridine 3

Compound **2** (0.31 g, 0.79 mmol) was stirred with aq trifluoroacetic acid (70%, 10 mL) at room temperature. After 3 h, the acid was evaporated under reduced pressure, co-evaporated with toluene (2 × 10 mL) and the residue was chromatographed to obtain compound **3** (0.17 g, 59%). [Eluent: 15–40% of MeOH in $CHCl_3$]. Hygroscopic solid. ^{1}H NMR (DMSO-d_6): δ 1.47–1.55 (m, 2H), 1.73–1.76 (m, 2H), 2.03–2.16 (m, 3H), 2.45–2.48 (m, 1H), 2.60–2.65 (m, 1H), 2.77–2.86 (m, 2H), 3.80–3.89 (m, 2H), 3.99–4.02 (m, 1H), 5.61 (d, J = 8.0 Hz, 1H), 5.69 (d, J = 4.0 Hz, 1H), 7.82 (d, J = 8.0 Hz, 1H), 11.34 (br s, 1H). ^{13}C NMR (DMSO-d_6): δ 28.6 (CH_2), 40.8, 53.7 (CH_2), 53.9 (CH_2), 60.0 (CH_2), 71.4, 73.1, 81.9, 89.3, 102.1, 141.7, 150.9 (C), 163.5 (C), 177.2 (C). HRMS (ES^+), m/z calcd for $(M+H)^+$ $C_{15}H_{22}N_3O_7$: 356.1458, found: 356.1457.

4.1.4. 5′-Deoxy-5′-N-(ethyl isonipecotatyl)thymidine 5

A mixture of 5′-*O*-tosylthymidine **4**[19] (0.80 g, 2.0 mmol) and neat ethyl *iso*nipecotate (6 mL) was heated at 60 °C. After 24 h, the reaction mixture was cooled to room temperature and poured into petroleum ether (50 mL) with stirring and the liquid was decanted. The residue was dissolved in 2–3 mL MeOH. It was then preadsorbed onto silica gel, applied on the top of the silica gel column, and chromatographed to obtain compound **5** (0.58 g, 76%). [Eluent: 0–8% of MeOH in $CHCl_3$]. Hygroscopic solid. ^{1}H NMR (D_2O): δ 1.24 (t, J = 7.2 Hz, 3H), 1.69–1.78 (m, 2H), 1.89 (s, 3H), 1.95–2.01 (m, 2H), 2.30–2.52 (m, 5H), 2.76–2.91 (m, 2H), 3.06–3.09 (m, 2H), 4.08–4.19 (m, 3H), 4.27–4.31 (m, 1H), 6.19–6.22 (m, 1H), 7.47 (s, 1H). ^{13}C NMR (D_2O + DMSO-d_6): δ 13.2, 15.0, 28.1 (CH_2), 39.2 (CH_2), 41.2, 53.6 (CH_2), 53.9 (CH_2), 61.3 (CH_2), 63.1 (CH_2), 73.9, 83.9, 86.8, 112.7 (C), 139.2, 152.9 (C), 167.7 (C), 178.6 (C). HRMS (ES^+), m/z calcd for $(M+H)^+$ $C_{18}H_{28}N_3O_6$: 382.1980, found: 382.1984.

4.1.5. 5′-Deoxy-5′-N-(4-carboxypiperidinyl)thymidine 6

Compound **5** (0.45 g, 1.14 mmol) was converted to compound **6** (0.26 g, 66%) following the procedure described for compound **2**. [Eluent: 5–20% of MeOH in $CHCl_3$]. Hygroscopic solid. ^{1}H NMR (DMSO-d_6): δ 1.47–1.56 (m, 2H), 1.73–1.83 (m, 5H), 1.95–2.17 (m, 5H), 2.39–2.67 (m, 2H), 2.81–2.84 (m, 2H), 3.80–3.83 (m, 1H), 4.08–4.11 (m, 1H), 6.10 (t, J = 6.8 Hz, 1H), 7.61 (s, 1H), 11.29 (br s, 1H). ^{13}C NMR (DMSO-d_6): δ 12.6, 28.7 (CH_2), 28.8 (CH_2),

38.8 (CH_2), 41.4, 53.7 (CH_2), 53.9 (CH_2), 60.5 (CH_2), 72.2, 84.2, 84.3, 109.9 (C), 136.5, 150.8 (C), 164.2 (C), 177.6 (C). HRMS (ES^+), *m*/*z* calcd for $(M+H)^+$ $C_{16}H_{24}N_3O_6$: 354.1665, found: 354.1669.

4.1.6. 2,3′-O-Anhydro-5′-deoxy-5′-N-(ethyl isonipecotatyl)thymidine 7

Compound **7** was prepared according to the reported procedure.[20] White solid. Mp: 230–232 °C (lit.[20] Mp: 230 °C).

4.1.7. 1-[2,5-Dideoxy-5-(4-carboxypiperidinyl)-β-D-threo-pentofuranosyl]thymine 8

Compound **7** (0.40 g, 1.10 mmol) was converted to compound **8** (0.25 g, 64%) following the procedure described for compound **2**. [Eluent: 5–20% of MeOH in $CHCl_3$]. Hygroscopic solid. ^1H NMR (DMSO-d_6): δ 1.74 (br s, 5H), 1.82–1.91 (m, 3H), 2.31–2.34 (m, 1H), 2.51–2.59 (m, 3H), 2.64–2.70 (m, 1H), 2.94–3.22 (m, 3H), 4.16 (br s, 1H), 4.22–4.23 (m, 1H), 6.06–6.09 (m, 1H), 7.79 (s, 1H), 11.26 (br s, 1H). ^{13}C NMR (DMSO-d_6): δ 12.9, 26.5 (CH_2), 38.9, 40.4 (CH_2), 52.1 (CH_2), 52.5 (CH_2), 56.9 (CH_2), 70.0, 79.7, 83.9, 109.4 (C), 137.6, 150.9 (C), 164.2 (C), 176.0 (C) HRMS (ES^+), *m*/*z* calcd for $(M+H)^+$ $C_{16}H_{24}N_3O_6$: 354.1665, found: 354.1674.

4.1.8. 5′-O-p-Tolylsulfonyl-2′,3′-didehydro-3′-deoxythymidine 9

Compound **9** was prepared according to the reported procedure.[22] White solid. Mp: 140 °C, dec. (lit.[22] Mp: 138 °C, dec.).

4.1.9. 5′-N-(Ethyl isonipecotatyl)-2′,3′-didehydro-3′,5′-dideoxythymidine 10

A mixture of 5′-*O*-tosyl D_4T **9** (0.80 g, 2.20 mmol) and neat ethyl *iso*nipecotate (8 mL) was heated at 60 °C. After 24 h, the reaction mixture was cooled to room temperature and diluted with EtOAc (50 mL). The EtOAc layer was washed with 10% $NaHCO_3$ solution (3 × 20 mL), separated, dried over anhyd Na_2SO_4 and filtered. The filtrate was evaporated to dryness and the residue purified over a silica gel column to afford compound **10** (0.66 g, 86%). [Eluent: 90–100% of EtOAc in petroleum ether]. Brown gum. ^1H NMR ($CDCl_3$): δ 1.19 (t, J = 7.2 Hz, 3H), 1.67–1.78 (m, 2H), 1.83–1.86 (m, 5H), 2.08–2.27 (m, 3H), 2.50–2.65 (m, 2H), 2.89–2.99 (m, 2H), 4.07 (q, J = 14.4 Hz, 2H), 4.94 (s, 1H), 5.75 (d, J = 5.6 Hz, 1H), 6.27 (d, J = 5.6 Hz, 1H), 6.95 (d, J = 2 Hz, 1H), 7.13 (s, 1H), 10.10 (br s, 1H). ^{13}C NMR ($CDCl_3$): δ 12.5, 14.1, 27.7 (CH_2), 27.8 (CH_2), 40.6, 53.4 (CH_2), 60.3 (CH_2), 62.2 (CH_2), 84.2, 89.9, 110.9 (C), 125.7, 135.6, 135.7, 150.9 (C), 164.2 (C), 174.8 (C). HRMS (ES^+), *m*/*z* calcd for $(M+H)^+$ $C_{18}H_{25}N_3O_5$: 364.1872, found: 364.1870.

4.1.10. 5′-N-(4-Carboxypiperidinyl)-2′,3′-didehydro-3′,5′-dideoxythymidine 11

Compound **10** (0.27 g, 0.73 mmol) was converted to compound **11** (0.18 g, 72%) following the procedure described for compound **2**. [Eluent: 5–15% of MeOH in $CHCl_3$]. Hygroscopic solid. ^1H NMR (DMSO-d_6): δ 1.49–1.55 (m, 2H), 1.71–1.74 (m, 2H), 1.78 (s, 3H), 1.97–2.10 (m, 3H), 2.40–2.45 (m, 1H), 2.60–2.64 (m, 1H), 2.75–2.87 (m, 2H), 4.85 (s, 1H), 5.89 (d, J = 6.0 Hz, 1H), 6.45 (d, J = 6.0 Hz, 1H), 6.77–6.78 (m, 1H), 7.34 (s, 1H), 11.40 (br s, 1H). ^{13}C NMR (DMSO-d_6): δ 12.6, 28.6 (CH_2), 41.1, 53.8 (CH_2), 54.3 (CH_2), 62.2 (CH_2), 85.1, 89.7, 109.9 (C), 125.5, 136.4, 136.5, 151.2 (C), 164.2 (C), 177.3 (C). HRMS (ES^+), *m*/*z* calcd for $(M+H)^+$ $C_{16}H_{22}N_3O_5$: 336.1559, found: 336.1551.

4.2. Biology

4.2.1. General methods

Bovine pancreatic RNase A, yeast tRNA, 2′, 3′-cCMP, 3′-CMP and human serum albumin (HSA) were purchased from Sigma–Aldrich. UV–vis measurements were made using a Perkin–Elmer UV–vis spectrophotometer (Model Lambda 25). Concentrations of the solutions were estimated spectrophotometrically using the following data: $\varepsilon_{278.5}$ = 9800 M^{-1} cm^{-1} (RNase A)[25] and ε_{268} = 8500 M^{-1} cm^{-1} (2′,3′-cCMP).[26]

4.2.2. Agarose gel-based assay

(i) Inhibition of RNase A was assayed qualitatively by the degradation of tRNA in an agarose gel. In this method, 20 μL of RNase A (1.26 μM) was mixed with 20 (0.09 mM), 40 (0.18 mM), and 60 μL (0.27 mM) of compounds **3**, **6**, **8**, and **11** separately to a final volume of 100 μL and the resulting solutions incubated for 3 h. 20 μL aliquots of the incubated mixtures were then mixed with 20 μL of tRNA solution (5.0 mg/mL tRNA, freshly dissolved in RNase free water) and incubated for another 30 min. Then 10 μL of sample buffer (containing 10% glycerol and 0.025% bromophenol blue) was added to this mixture and 15 μL from each solution was extracted and loaded onto a 1.1% agarose gel. The gel was run using 0.04 M Tris–acetic acid–EDTA (TAE) buffer (pH 8.0). The residual tRNA was visualized by ethidium bromide staining under UV light.

(ii) Inhibition of RNase A by compounds **2** and **3** were assayed qualitatively by the degradation of tRNA in a comparative agarose gel. In this method, 20 μL of RNase A (1.26 μM) was mixed with 20 (0.09 mM), 40 (0.18 mM), and 60 μL (0.27 mM) of compound **2** and 40 (0.18 mM) and 60 μL (0.27 mM) of compound **3** separately and the resulting solutions incubated for 3 h. Then gel was run according to the method described above and the residual tRNA was visualized after ethidium bromide staining under UV light.

4.2.3. Precipitation assay with RNase A

Inhibition of the ribonucleolytic activity of RNase A was quantified by the precipitation assay as described by Bond.[27] In this method 10 μL of RNase A (1.26 μM) was mixed with 40 μL of compounds **3**, **6**, **8**, and **11** (0.27 mM) individually to a final volume of 100 μL and incubated for 2 h at 37 °C. Twenty microliters of the resulting solutions from the incubated mixtures were then mixed with 40 μL of tRNA (5 mg/mL tRNA freshly dissolved in RNase A free water), 40 μL of Tris–HCl buffer of pH 7.5 containing 5 mM EDTA and 0.5 mg/mL HSA. After incubation of the reaction mixture at 25 °C for 30 min, 200 μL of ice-cold 1.14 (M) perchloric acid containing 6 mM uranyl acetate was added to quench the reaction. The solution was then kept in ice for another 30 min and centrifuged at 4 °C at 12,000 rpm for 5 min. Fifty microliters of the supernatant was taken and diluted to 1 mL. The decrease in absorbance at 260 nm was measured and compared to a control set.

4.2.4. Inhibition kinetics with RNase A

(i) *By Dixon plot:* The inhibition of RNase A by compounds **3**, **6**, and **8** were assessed individually by a spectrophotometric method as described by Anderson et al.[26] The assay was performed in 0.1 M Mes-NaOH buffer, pH 6.0 containing 0.1 M NaCl using 2′,3′-cCMP as the substrate. The inhibition constants (K_i) were calculated from initial velocity data. The reciprocal of initial velocity was plotted against the inhibitor concentration (Dixon Plot) according to Eq. (1):

$$\frac{1}{v} = \frac{K_m}{V_{max}[S]K_i}[I] + \frac{1}{V_{max}}\left[1 + \frac{K_m}{[S]}\right] \quad (1)$$

where, v is the initial velocity, [S] the substrate concentration, [I] the inhibitor concentration, K_m the Michaelis constant, K_i the inhibition constant, and V_{max} the maximum velocity.

(ii) *By Lineweaver–Burk plot:* The inhibition of RNase A by compounds **3**, **6**, **8**, and **11** were assessed individually by a spectrophotometric method as described by Anderson et al.[26] The assay was performed in 0.1 M Mes-NaOH buffer, pH 6.0 containing 0.1 M

NaCl using 2′,3′-cCMP as the substrate. The inhibition constants were calculated from initial velocity data using Lineweaver–Burk plot. For the Lineweaver–Burk plot the reciprocal of initial velocity was plotted against the reciprocal of substrate concentration at a constant inhibitor concentration according to the above Eq. (1). The kinetics experiments were performed with two fixed inhibitor concentrations and another in absence of inhibitor with varying substrate (2′,3′-cCMP) concentrations. The slopes from the double reciprocal plot were again replotted against the corresponding inhibitor concentrations to get inhibition constants (K_i).

4.2.5. FlexX docking

The crystal structure of the protein 1FS3 (PDB entry for RNase A) was downloaded from the Protein Data Bank.[28] Water molecules and other ions present in the crystal structures were subtracted to prepare the protein PDB file for docking. The 3D structures of compounds **3**, **6**, **8**, and **11** were generated in SYBYL6.92 (Tripos Inc., St. Louis, USA) and their energy-minimized conformations were obtained with the help of the MMFF94 force field with all other default parameters. The *FlexX* software as part of the SYBYL suite was used for docking of the ligands to the protein. The ranking of the generated solutions was performed using a scoring function that estimates the free binding energy (ΔG) of the protein–ligand complex considering specific types of molecular interactions as described in Rarey et al.[29] Each docked conformation is looked upon as a possibility of how the ligand may bind with the protein. We have chosen the pose with the minimum score for the docked conformation for each inhibitor molecule. *PyMol*[30] was used for visualization of the docked conformations. The theoretical energy calculation of the docked structures of the protein–ligand complexes was computed using *PEARLS*[24] which gives the interaction energies for receptor ligand systems based on molecular-mechanics-based energy functions.[31]

Acknowledgments

A.S. thanks the Council of Scientific and Industrial Research, New Delhi, India for a fellowship. The Department of Science and Technology (DST), New Delhi, India is thanked for the creation of 400 MHz facility in the Department of Chemistry, Indian Institute of Technology Kharagpur, India under IRPHA program.

Supplementary data

Supplementary data associated with this article can be found, in the online version, at doi:10.1016/j.bmc.2010.08.059.

References and notes

1. Riordan, J. F. In *Ribonucleases: Structures and Functions*; D'Alessio, G., Riordan, J. F., Eds.; Academic Press: New York, 1997; p 445.
2. D'Alessio, G.; di Donato, A.; Mazzarella, L.; Piccoli, R. In *Ribonucleases: Structures and Functions*; D'Alessio, G., Riordan, J. F., Eds.; Academic Press: New York, 1997; p 383.
3. D'Alessio, G. *Trends Cell Biol.* **1993**, *3*, 106.
4. Shapiro, R.; Riordan, J. F.; Vallee, B. L. *Biochemistry* **1986**, *25*, 3527.
5. D'Alessio, G.; di Donato, A.; Parente, L.; Piccoli, R. *Trends Cell Biol.* **1991**, *16*, 104.
6. Shapiro, R.; Vallee, B. L. *Biochemistry* **1989**, *28*, 7401.
7. Sorrentino, S.; Glitz, D. G.; Hamann, K. J.; Loegering, D. A.; Checkel, J. L.; Gleich, G. J. *J. Biol. Chem.* **1992**, *267*, 14859.
8. Yakovlev, G. I.; Mitkevich, V. A.; Makarov, A. A. *Mol. Biol.* **2006**, *40*, 867.
9. Raines, R. T. *Chem. Rev.* **1998**, *98*, 1045.
10. Russo, N.; Acharya, K. R.; Shapiro, R. *Methods Enzymol.* **2001**, *341*, 629.
11. Russo, N.; Shapiro, R. *J. Biol. Chem.* **1999**, *274*, 14902.
12. Herries, D. G.; Mathias, A. P.; Rabin, B. R. *Biochem. J.* **1962**, *85*, 127.
13. Maiti, T. K.; De, S.; Dasgupta, S.; Pathak, T. *Bioorg. Med. Chem.* **2006**, *14*, 1221.
14. Fisher, B. M.; Schultz, L. W.; Raines, R. T. *Biochemistry* **1998**, *37*, 17386.
15. Debnath, J.; Dasgupta, S.; Pathak, T. *Bioorg. Med. Chem.* **2009**, *17*, 4921.
16. Debnath, J.; Dasgupta, S.; Pathak, T. *Bioorg. Med. Chem.* **2009**, *17*, 6491.
17. Leonidas, D. D.; Maiti, T. K.; Samanta, A.; Dasgupta, S.; Pathak, T.; Zographos, S. E.; Oikonomakos, N. G. *Bioorg. Med. Chem.* **2006**, *14*, 6055.
18. Samanta, A.; Leonidas, D. D.; Dasgupta, S.; Pathak, T.; Zographos, S. E.; Oikonomakos, N. G. *J. Med. Chem.* **2009**, *52*, 932.
19. Reist, E. J.; Benitez, A.; Goodman, L. *J. Org. Chem.* **1964**, *29*, 554.
20. Sakthivel, K.; Kumar, R. K.; Pathak, T. *Tetrahedron* **1993**, *49*, 4365.
21. Cosford, N. D. P.; Schinazi, R. F. *J. Org. Chem.* **1991**, *56*, 2161.
22. Adachi, T.; Yamada, Y.; Inoue, I. *Carbohydr. Res.* **1979**, *73*, 113.
23. Purich, D. L.; Fromm, H. J. *Biochim. Biophys. Acta* **1972**, *268*, 1.
24. Han, L. Y.; Lin, H. H.; Li, Z. R.; Zheng, C. J.; Cao, Z. W.; Xie, B.; Chen, Y. Z. *J. Chem. Inf. Model.* **2006**, *46*, 445.
25. Sela, M.; Anfinsen, C. B. *Biochim. Biophys. Acta* **1957**, *24*, 229.
26. Anderson, D. G.; Hammes, G. G.; Walz, F. G. *Biochemistry* **1968**, *7*, 1637.
27. Bond, M. D. *Anal. Biochem.* **1988**, *173*, 166.
28. Berman, H. M.; Westbrook, J.; Feng, Z.; Gilliland, G.; Bhat, T. N.; Weissig, H.; Shindyalov, I. N.; Bourne, P. E. *Nucleic Acids Res.* **2000**, *28*, 235.
29. Rarey, M.; Kramer, B.; Lengauer, T.; Klebe, G. *J. Mol. Biol.* **1996**, *261*, 470.
30. DeLano, W. L. The PyMOL Molecular Graphics System, DeLano Scientific, San Carlos, CA, USA. 2006. http://pymol.sourceforge.net/.
31. Hydrogen bonding distances are available in Tables S1 and S2 in Supplementary data.